PHYSICAL REVIEW E VOLUME 57, NUMBER 2 FEBRUARY 1998

Binary random cellular structures

G. Schliecker
Max-Planck-Institut für Physik Komplexer Systeme, D-01187 Dresden, Germany
(Received 2 June 1997)

A topological model for binary random cellular structures under neighbor-switching is presented. Performing exact analytical calculations, one obtains a bimodal cell shape distribution, whereas Aboav's law for the correlations between neighboring cells holds for each species separately. The binary character of the tessellation is reduced with increasing disorder. The calculated topological properties are analyzed in comparison with recent experimental studies of binary disc assemblies on an air table. [S1063-651X(98)51402-X]

PACS number(s): 05.40.+j, 05.90.+m, 64.60.−i

Recent thorough experimental and theoretical work has been devoted to the universal topological properties of two-dimensional random cellular structures [1–5], focusing on the cell shape distribution and on the correlations between neighboring cells. The cell shape distribution is denoted as $\{p_k\}$, where p_k is the probability that a randomly chosen cell has k sides. In most natural random mosaics, $\{p_k\}$ is a narrow distribution peaked at $k=6$, the average number of sides of the cells in mosaics with trivalent vertices. Correlations between neighboring cells are usually investigated by means of the quantity $km(k)$, the average total number of sides of the neighbors of a k-sided cell. An empirical law [2] states that this quantity varies linearly in k. These observations have been confirmed in detailed experimental studies of the Laguerre-tessellations of mono-size disc arrangements on an air table [3]. Moreover the universal behavior of the cell shape distribution, first noticed in [6], has been established. Through slight inhomogeneities of the table, the discs rearrange permanently and statistical equilibrium is achieved. For random tessellations in statistical equilibrium, froths, maximum entropy inference yields the empirically determined laws [1,7].

In arrangements of discs with two different sizes on the air table, however, the topological properties of the tessellations change drastically [8]. At high packing fraction, one observes bimodal cell shape distributions, and $km(k)$ for the whole tessellation is no longer linear. The experimental results imply that Aboav's law [2] holds instead for the neighbors of each species separately. These effects are less pronounced, when the density is reduced, and for vanishing density the patterns of two species are indistinguishable. Aboav's law for binary assemblies is consistent with the maximum-entropy theory [9], but so far no topological model has been presented yet which may be applied to these systems.

Formulating a topological model for a dynamical tessellation, only those geometrical changes which affect the number of sides of cells, the topological transformations, are of importance. In two-dimensional systems of moving discs, the T1-transformation (neighbor switching) is the dominant process (see Fig. 1). Clearly, the possibility for such a process is severely constrained in a dense packing. But even at vanishing density, the topological dynamics turn out to be restricted. In this case, the air table tessellations converge to the Poisson-Voronoi-tessellation, which is far away from theoretically obtained structures, in which the neighbor-switching occurs with minimal restrictions [10,11]. The topological properties of mono-size disc assemblies on the air table are very similar to those of a model introduced by Le Caër [12], in which the possibilities for T1 transformations are severely restricted. In order to make the connection between this model and the experiments, we consider the structure represented in Fig. 2(a) as a dynamical network, in which the neighbor switching randomly occurs at the dashed edges. Weighing the probability for the flip of a randomly chosen dynamical edge with p if it is in the position of Fig. 2(a) and with $1-p$ for the reverse process, the statistical equilibrium properties coincide with the solution of Le Caër's model [12]. Comparing theoretical and experimental results and interpreting the parameter $w=|1-2p|$ as a measure of the packing fraction, one obtains an excellent agreement for dense packings. Clearly, the melting transition accompanied by a change of slopes in $km(k)$ and the occurrence of triangles or cells with more than eight sides are out of the scope of this theoretical approach. Nevertheless, even in the low-density limit, this model still gives a fair fit of the local topological ordering in the disc system.

Following this line, a simple model for binary random cellular structures will be derived. Since in the limit of vanishing density of discs all tessellations converge to the same structure, we require the low-density limit of our model to be identical with the model in [12] at $p=1/2$ and this way choose the arrangement of dynamical and fixed edges. In order to obtain the transition from highest packing fraction to vanishing density, the dynamics are defined as follows: The probabilities for the T1 transformations are chosen to be independent and weighted with p for the transformation on

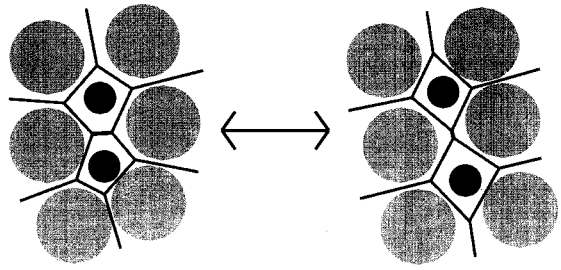

FIG. 1. Neighbor switching in a random packing of discs.

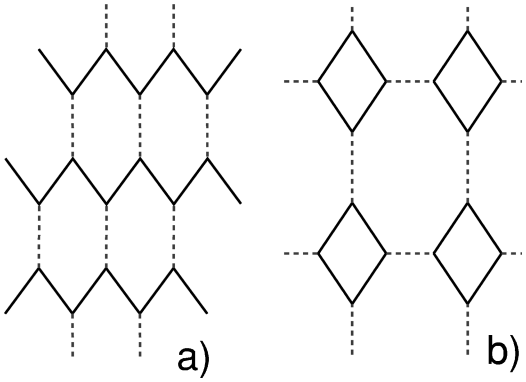

FIG. 2. The dense packing structures of (a) the model in [12] and (b) the model for a binary random structure. Dashed edges may, straight edges can never perform a T1 transformation.

dynamical edges, which are in their position of the dense packing structure, and with $1-p$ for the reverse process. The dense packing structure of the discs on the air table in general depends on the percentage and the size ratio of the two kinds of discs. The latter corresponds to the average numbers of sides of the two classes of cells of the equivalent Laguerre-tessellations. The simplest choice for such a tessellation is the regular lattice represented in Fig. 2(b), which can be subdivided into two equally weighted structures, one of which is built up by quadrilaterals $(-)$ and the other by octaeder $(+)$, corresponding to the Laguerre cells of small and large discs, respectively. The T1 transformations are restricted to the dashed edges. A possible realization of the disordered structure is represented in Fig. 3. The dotted edges are flipped with respect to their position in Fig. 2(b) as result of a T1 transformation with probability p.

Through the dynamics, the topological quantities converge to their stationary values. Consider a set of N dynamical edges, where $\Pi_l(p,N)$ is the probability that l of them

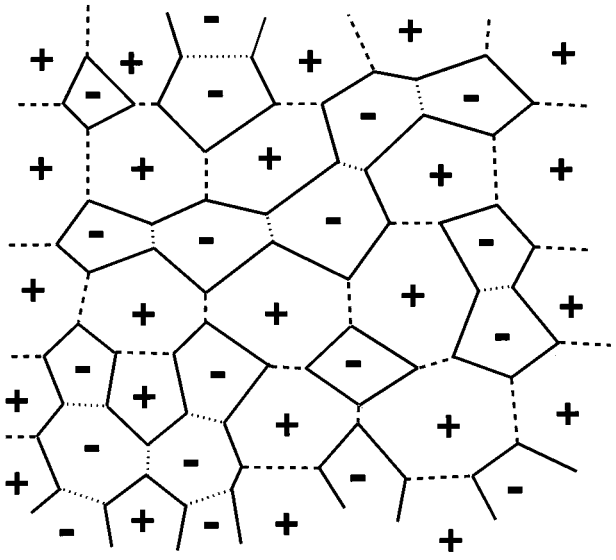

FIG. 3. Possible realization of a disordered structure. The dashed edges are in the state of Fig. 2(b), the dotted edges are flipped with respect to this state.

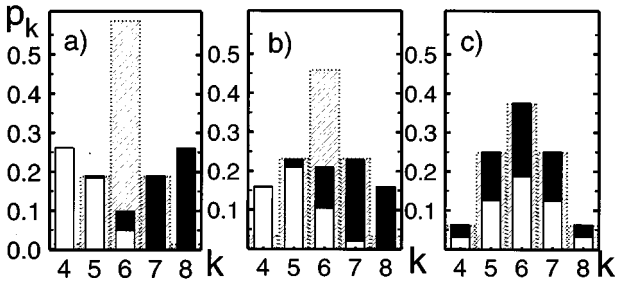

FIG. 4. Cell shape distributions for (a) $w=0.7$, (b) $w=0.5$, and (c) $w=0$. The contributions from the quadrilaterals (octaeder) are represented as white (black) bars. Grey bars represent the distribution of Le Caër's model [12].

are flipped with respect to their initial position. Choosing randomly an edge and applying a T1 transformation with probability p to the edges which are in their initial position and with $1-p$ to the flipped edges, the average change of Π_l for fixed p and N is given by $\Delta\Pi_l=\beta_{l-1}\Pi_{l-1}-\alpha_l\Pi_l+\alpha_{l+1}\Pi_{l+1}-\beta_l\Pi_l$, where $\alpha_l=(1-p)l/N$ and $\beta_l=p(N-l)/N$. Repeating this procedure at a constant rate in time and performing the transition to the continuous time representation, it is not too hard to see that Π_l approaches exponentially its unique stationary solution, which is a binomial distribution:

$$\Pi_l(p,N)=\binom{N}{l}p^l(1-p)^{N-l}. \tag{1}$$

In order to determine the stationary cell shape distribution of our model, it is convenient to study the contributions of the substructures separately. We define $p_k^{(s)}$ as the probability that a randomly chosen cell from the structure s, $s=\pm$, has k sides. Through the dynamics, each cell can be affected by four dynamical edges. The quadrilaterals represented in Fig. 2(b) gain one side per flip of these edges, the octaeder lose one side. Thus, making use of the result (1), we obtain the stationary solutions

$$p_k^{(s)}(w)=\Pi_{k-4}(w_s,4), \tag{2}$$

with $w_s=(1+sw)/2$ and $w=1-2p$. The total distribution, obtained from $p_k=(p_k^{(+)}+p_k^{(-)})/2$, is represented in Fig. 4 for three different values of w. The symmetry of the problem allows one to discuss the case $0\leqslant w\leqslant 1$ exclusively. For large w, the cells with less than six sides almost exclusively belong to the $(-)$ structure. With decreasing w, the binary character is reduced. At $w=0$, the two subdistributions in Eq. (2) are indistinguishable. This is exactly what is observed on the air table [8], if we interpret the parameter w as a measure of the packing fraction. Our choice of the dense structure in Fig. 2(b) fixes a different size ratio than discussed in [8], and thus a quantitative comparison cannot be performed.

In order to determine $km(k)$, we consider the neighbors of each species separately. Each s cell has four *fixed* neighbors. They are exclusively $(-s)$ cells; see Figs. 2(b) and 3. Their average total number of sides is denoted as $4f_k^{(-s)}$. The remaining $(k-4)$ *dynamical* neighbors belong to the

same class as the central cell, their total number of sides is in average $(k-4)d_k^{(s)}$. In this notation, the total number of sides of cells adjacent to a k-sided cell from species s reads

$$km^{(s)}(k)=4f_k^{(-s)}+(k-4)d_k^{(s)}. \tag{3}$$

The averages can be easily calculated. Keeping in mind that the average of $4f_k^{(s)}$ just counts four times the average number of sides of s cells, we obtain $\Sigma_k 4f_k^{(-s)}p_k^{(s)}=4\langle k\rangle^{(-s)}$ with $\langle k\rangle^{(s)}=\Sigma_k kp_k^{(s)}$. The average number of sides of the dynamical neighbors of one species is obtained with a similar argument:

$$\sum_k (k-4)d_k^{(s)}p_k^{(s)}=\langle k-4\rangle^{(s)}\langle k\rangle^{(s)}+\mu_2^{(s)}, \tag{4}$$

where the variance of $p_k^{(s)}$ is denoted as $\mu_2^{(s)}=\langle(k-\langle k\rangle^{(s)})^2\rangle$. Consider now the dynamical edges of the fixed neighbors. Each fixed neighbor cell may be affected simultaneously with the central cell by the flips of two dynamical edges. If one of these edges is flipped, k is lowered or raised by 1, and the four fixed neighbors in common gain or lose two edges. The remaining dynamical edges are disconnected from the central cell and flip independently. Thus, in statistical equilibrium, their arrangement does not depend on k, and we can summarize,

$$4f_k^{(s)}-4f_{k-1}^{(s)}=-2. \tag{5}$$

The number of sides of each dynamical neighbor depends on the configuration of its three dynamical edges, which are disconnected from the central cell. Since their contributions to all dynamical neighbor cells are identical, $d_k^{(s)}$ does not depend on k. Making use of Eq. (4), we obtain $d_k^{(s)}=d^{(s)}=\langle k\rangle^{(s)}+\mu_2^{(s)}/\langle k-4\rangle^{(s)}$. Putting it all together, Eq. (3) reads

$$km^{(s)}(k)=(d^{(s)}-2)(k-4)+40-2\langle k\rangle^{(s)}, \tag{6}$$

which is in agreement with the experimental observation of two linear $km^{(s)}(k)$. The same result can be obtained as well by making use of the microreversibility argument, introduced in [10]. The full contribution is given by $km(k)p_k=km^{(+)}(k)p_k^{(+)}+km^{(-)}(k)p_k^{(-)}$.Due to the different behavior of the subdistributions $p_k^{(\pm)}$ for nonvanishing w, the contribution of $km^{(-)}(k)$ is dominant for $k<6$, whereas for large cells $km^{(+)}(k)$ plays the important role. Since for $w\neq 0$ these two contributions differ, $km(k)$ is no longer linear in k. The two contributions and the full $km(k)$ are represented in Fig. 5 for the extreme cases: $w\approx 1$ (a), for which the differences are largest, and $w=0$(b), for which the $km^{(s)}(k)$ are identical. The difference in slopes in Eq. (6) is not confirmed by the published experimental results. It follows from the dense packing structure represented in Fig. 2(b), chosen here for its simplicity and its uniqueness, at a size ratio, which is the highest possible within the framework of our approach. For this choice, all dynamical neighbors are part of the same class as the central cell, yielding the large difference in slopes in Eq. (6). Also the relative arrangement of the two different kinds of cells in this case turns out to be different from those observed in detailed studies of random packings [13]. Especially, the choice in Fig. 2(b) disables the random arrangement of (+) and (–) cells, which is to be expected at vanishing density. Also, the maximum possible value of 2/3 for the fraction of edges separating mixed neighbors, which is obtained here for all values of w, is not achieved in experimental tessellations [13]. A better reproduction of the experimentally observed arrangements can be obtained at smaller differences in size, for which the dense packing structures turn out to be less restricted within the framework of our approach. This fact allows the construction of less regular, more realistic high density arrangements of the two kinds of cells converging to the random limit at $w=0$. The generalization of our calculations to such more complicated structures at $w=1$ is straightforward though technically more involved.

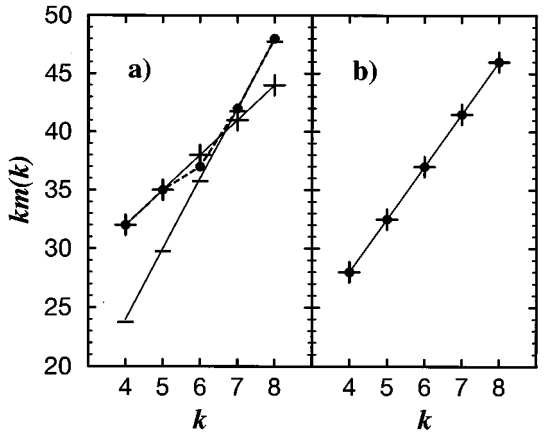

FIG. 5. $km(k)$ for (a) $w\approx 1$ and (b) $w=0$. The values of $km^{(+)}(k)$ and $km^{(-)}(k)$ are represented as (+) and (−); black circles represent the total contribution $km(k)$.

Summarizing, within the framework of the simple topological model presented here some of the striking topological properties of binary random cellular structures could be obtained. Comparing our results with experimental data for tessellations of binary disc assemblies on the air table [8], we find a satisfactory agreement with the qualitative properties of the cell shape distribution and also obtain two linear $km^{(s)}(k)$. A realistic arrangement of the cells of the two different kinds of discs, however, can only be achieved for more complicated dense packing structures than that one chosen here. The investigation of these structures and their generalization to different size ratii and arbitrary percentages of the two kinds of cells are left to future work.

The author is grateful to V. Sperling, M. Lorenz, H. Hinrichsen, and D. Stoyan for numerous valuable discussions.

[1] N. Rivier, in *Disorder and Granular Media*, edited by D. Bideau and A. Hansen (Elsevier Science Publishers, B. V., 1993), p. 77.
[2] D. A. Aboav, Metallography **3**, 383 (1970).
[3] J. Lemaître, J. P. Troadec, A. Gervois, and D. Bideau, Europhys. Lett. **14**, 77 (1991); J. Lemaître, A. Gervois, J. P. Troadec, N. Rivier, M. Ammi, L. Oger, and D. Bideau, Philos. Mag. B **67**, 347 (1993).
[4] R. Delannay and G. Le Caër, Phys. Rev. Lett. **73**, 1553 (1994).
[5] U. Thiele and K. Nitschke (unpublished).
[6] G. Le Caër, J. Phys. A **24**, 4655 (1991).
[7] N. Rivier, in *From Statistical Inference and Back*, edited by P. Grassberger and J. P. Nadal (Kluwer, Dordrecht, 1994), p. 77.
[8] C. Annic, J. P. Troadec, A. Gervois, J. Lemaître, M. Ammi, and L. Oger, J. Phys. (France) I **4**, 115 (1994).
[9] N. Rivier, J. Phys. (France) I **4**, 127 (1994).
[10] M. A. Peshkin, K. Strandburg, and N. Rivier, Phys. Rev. Lett. **67**, 1803 (1991).
[11] C. Godrèche, I. Kostov, and I. Yekutieli, Phys. Rev. Lett. **69**, 2674 (1992).
[12] G. Le Caër, J. Phys. A **24**, 1307 (1991).
[13] J. P. Troadec, A. Gervois, C. Annic, and J. Lemaître, J. Phys. (France) I **4**, 1121 (1994).